Journal of Alloys and Compounds 509 (2011) 1517–1522

Contents lists available at ScienceDirect

Journal of Alloys and Compounds

journal homepage: www.elsevier.com/locate/jallcom

Synthesis and structure determination of $In_3TeO_3F_7$: An indium oxyfluorotellurate IV derived from W bronze structure with Te^{4+} in hexagonal tunnels

N. Jennene Boukharrata*, J.P. Laval

Laboratory of «Science des Procédés Céramiques et de Traitements de Surface», UMR-CNRS n° 6638, Limoges University, 123, Avenue A. Thomas, 87060 Limoges Cedex, France

ARTICLE INFO

Article history:
Received 8 July 2010
Received in revised form 17 October 2010
Accepted 27 October 2010
Available online 2 November 2010

Keywords:
Indium tellurium IV oxyfluoride
Crystal structure
Bronze structure
MIn_3F_{10} structure
Oxyfluorotellurate
Disorder

ABSTRACT

After $InTeO_3F$ and $InTe_2O_5F$ recently described, a new compound $In_3TeO_3F_7$ is characterized in the In–Te^{IV}–O–F system. The crystal structure was determined by single X-ray diffraction and refined to $R_1 = 0.028$. $In_3TeO_3F_7$ crystallizes in orthorhombic space group *Cmmm*, $a = 7.850(2)$ Å, $b = 27.637(6)$ Å, $c = 4.098(1)$ Å, $V = 889.1(4)$ Å^3 and $Z = 4$. Its structure consists of the stacking, *via* vertices, of identical layers composed of InF_6 and InO_2F_4 octahedra sharing corners and of InO_4F_3 pentagonal bipyramids sharing edges and vertices. The Te cations statistically occupy one or the other of two close sites located inside tunnels delimited by the In polyhedra and are bonded to F anions located in the same tunnels.

The structure can be considered as an intergrowth of parallel strips of MIn_3F_{10} and hexagonal tungsten bronze (c)-types. It is compared to other structures such as the bronze $Sb_{0.157}WO_3$, $TeMo_5O_{16}$ and $Sb_2Mo_{10}O_{31}$, phases also comprising Te^{4+} or Sb^{3+} inside hexagonal tunnels. The electronic lone pair of Te^{4+} is stereochemically active and a perfect O/F ordering occurs on the anionic sites.

1. Introduction

In recent years, a systematic investigation of oxyfluorotellurates(IV) has been started, in order to extend the field of materials likely to present interesting optical non-linear properties, reserved to oxides until now. Introducing an extra anion as F^-, acting as a modifier of tellurates IV environment, successively, new oxyfluorides, $TeOF_2$ [1] and $Te_2O_3F_2$ [2], oxyfluorotellurates: $MTeO_3F$ (M = Fe, Cr, Ga, In, Sc) [3,4], $V_2Te_2O_7F_2$ [5], $TiTeO_3F_2$ [5] and $InTe_2O_5F$ [6] have been synthesized and structurally characterized. In these last phases, the trivalent or tetravalent cation associated to tellurium IV is in octahedral coordination. Some of them being non-centrosymmetric, their Second Harmonic Generations (SHG) were studied.

The present work deals with another oxyfluorotellurate (IV): $In_3TeO_3F_7$, poorer in tellurium, and presenting different structural features from the previous phases, with Te^{4+} inserted inside tunnels. It is compared to a few numbers of phases of similar nature which can be gathered in a homogeneous structural family deriving from bronze type.

2. Experimental methods

2.1. Crystal synthesis

$In_3TeO_3F_7$ is obtained as a pure phase by a solid-state reaction using a mixture of 64 (mol%) InF_3–9 (mol%) In_2O_3–27 (mol%) TeO_2 heated in a platinum sealed tube. The composition seems strictly stoichiometric. However the single crystals used for this study are obtained from a slightly different composition: 71 (mol%) InF_3–29 (mol%) TeO_2. The refined lattice parameters are exactly the same as for the nominal composition.

InF_3 and In_2O_3 were commercial products (Aldrich, 99.9%). TeO_2 was prepared in the laboratory by decomposition at 823 K under flowing oxygen of commercial H_6TeO_6 (Aldrich, 99.9%). This process gives tellurium dioxide of a good quality and reactivity, without traces of moisture.

To obtain $In_3TeO_3F_7$ single crystals the following heat treatment is adopted: the temperature was progressively increased to 963 K (5° min^{-1}), held for 4 days, then slowly decreased to 693 K (0.1° min^{-1}) and held for 2 days at this last temperature. Finally, the platinum tube was water-quenched to room temperature. Colourless and moisture-resistant tablets were obtained, grown in a more or less melted mixture. Many were twinned or cleaved. A second heat treatment was necessary: the product was crushed and heated a new time in a gold sealed tube. The temperature was progressively increased to 693 K (5° min^{-1}), held for 2 days and then decreased to

* Corresponding author. Tel.: +33 0668264231; fax: +33 0555457586.
E-mail address: nefla.boukharrata@unilim.fr (N. Jennene Boukharrata).

0925-8388/$ – see front matter © 2010 Elsevier B.V. All rights reserved.
doi:10.1016/j.jallcom.2010.10.139

Table 1
Crystal and structure refinement data.

Formula	$In_3TeO_3F_7$
Formula weight (g)	653.05
Temperature (K)	293
Crystal system	Orthorhombic, *Cmmm*
a (Å)	7.850(2)
b (Å)	27.637(6)
c (Å)	4.098(1)
Volume (Å^3)	889.1(4)
Z	4
d_{calc} (g cm^{-3})	4.879
μ (mm^{-1})	11.03
F(0 0 0)	1144
Crystal size (mm)	0.09 × 0.05 × 0.03
θ range (°)	5.19–27.47
Data collected	$-9 < h < 10$, $-35 < k < 35$, $-5 < l < 5$
Reflection collected/unique	5970/634
Refinement method	Full-matrix least-squares on F^2
Data/restraints/parameters	634/0/61
Goodness of fit on F^2	1.216
Final *R* indices [$I > 2\sigma(I)$]	$R_1 = 0.028$, $wR_2 = 0.053$
R indices (all data)	$R_1 = 0.045$, $wR_2 = 0.058$
Largest diff. peak and hole (e Å^{-3})	2.15 and −1.09

593 K (0.1° min^{-1}) and held for 4 days at this last temperature. Similar colourless tablets were obtained. They were suitable for X-ray diffraction study.

2.2. Structure solution and refinement

A single crystal of $In_3TeO_3F_7$ was selected, mounted on a tapered fibreglass, and placed on a Nonius Kappa CCD four circle diffractometer. Full space data were collected at room temperature using monochromatic Mo*Kα* radiation. Unit cell parameters were refined using *DIRAX/LSQ* [7] and data integrated with *EVALCCD* [8] programs.

The integrated intensities were corrected for absorption effects by using a multi-scan method: *SADABS* [9], lowering R_{int} from 0.088 to 0.042. Selected data collection parameters and crystallographic data are provided in Table 1.

The structure was solved by direct methods and refined on the basis of F^2 for all unique data using *SHELXS97* [10] and *SHELXL97* [10]. The refined atomic coordinates and anisotropic thermal parameters are listed in Tables 2 and 3 respectively. The selected interatomic distances for $In_3TeO_3F_7$ are given in Table 4.

The preliminary study of the diffraction pattern shows that some anomalies (cleavage, twinning, . . .) occur on most single crystals, whatever the thermal treatment is. Only slight improvements result from longer time or multiple annealing. The precession patterns perpendicular to the main axes show the presence of a strong and well defined orthorhombic C sublattice and of diffuse spots (Fig. 1) intercalated between the 1*kl*, 2*kl* and 3*kl* reciprocal planes of the sublattice and forming new 1.5*kl*, 2.5*kl* and 3.5*kl* diffuse planes. In these planes, the diffuse spots extend along [0 *k* 0] forming series of dashed lines, as shown in the representation of the 1.5*kl* reciprocal plane in Fig. 2. Similar observations have been made in many phases deriving from bronze-like types and generally result from short or medium range organisation of defects (interstitial cations) in tunnels. Considering the relative independence of the sublattice, the diffuse superstructure and also the great difficulty to define a plausible lattice parameter for the superlattice along [0 *k* 0], the present work consists in refining and describing the well-defined

Table 2
Atomic coordinates and equivalent isotropic displacement factors U_{eq} (Å^2) for $In_3TeO_3F_7$.

Atoms	*x*	*y*	*z*	U_{eq}
In1	0.5000	0.6237(1)	0.0000	0.0080(2)
In2	0.7652(1)	0.5000	0.0000	0.0070(3)
In3	0.7500	0.7500	0.0000	0.0113(3)
Te1	0.9434(4)	0.6059(1)	0.0000	0.0200(7)
Te2	0.9032(19)	0.6225(7)	0.0000	0.023(3)
O1	0.7051(7)	0.5781(2)	0.0000	0.0163(12)
O2	1.000	0.5424(3)	0.0000	0.035(3)
F1	0.7541(9)	0.5000	0.5000	0.0257(19)
F2	0.7500	0.7500	0.5000	0.034(2)
F3	0.5000	0.6275(3)	0.5000	0.0271(17)
F4	1.0000	0.7290(3)	0.0000	0.033(2)
F5	0.5000	0.5000	0.0000	0.032(3)
F6	0.6846(7)	0.6784(1)	0.0000	0.0276(13)
F7	0.929(3)	0.6143(8)	0.5000	0.005(5)
F8	1.0000	0.5962(17)	0.5000	0.005(5)

Table 3
Anisotropic displacement factors (Å^2) for $In_3TeO_3F_7$.

Atoms	U_{11}	U_{22}	U_{33}	U_{23}	U_{13}	U_{12}
In1	0.0071(4)	0.0096(4)	0.0073(4)	0.0000	0.0000	0.0000
In2	0.0059(5)	0.0088(4)	0.0064(4)	0.0000	0.0000	0.0000
In3	0.0120(5)	0.0120(4)	0.0099(5)	0.0000	0.0000	−0.0013(3)
Te1	0.0091(11)	0.0087(13)	0.0423(11)	0.0000	0.0000	−0.0019(8)
O2	0.008(4)	0.015(4)	0.082(9)	0.0000	0.0000	0.0000
F1	0.028(5)	0.039(4)	0.010(4)	0.0000	0.0000	0.0000
F2	0.053(6)	0.037(5)	0.010(4)	0.0000	0.0000	0.001(4)
F3	0.033(4)	0.043(4)	0.006(3)	0.0000	0.0000	0.0000
F4	0.013(4)	0.021(4)	0.065(6)	0.0000	0.0000	0.0000
F5	0.002(5)	0.056(7)	0.038(7)	0.0000	0.0000	0.0000
F6	0.023(3)	0.015(2)	0.045(4)	0.0000	0.0000	−0.011(2)

Table 4
Selected interatomic distances (Å) for $In_3TeO_3F_7$.

In1–O1^{ii}	2.045(6)	In3–F6^{vi}	2.044(4)
In1–O1	2.045(6)	In3–F6	2.044(4)
In1–F3^{iii}	2.052(1)	In3–F4^{vi}	2.047(2)
In1–F3	2.052(1)	In3–F4	2.047(2)
In1–F6^{ii}	2.095(5)	In3–F2^{iii}	2.0490(5)
In1–F6	2.095(5)	In3–F2	2.0490(5)
In2–F1^{iii}	2.051(1)	Te1–O2	1.810(9)
In2–F1	2.051(1)	Te1–O1	2.023(6)
In2–F5	2.082(1)	Te1–F7	2.065(3)
In2–O2^{v}	2.184(5)	Te1–F6	2.853(7)
In2–O2	2.184(5)	Te1–O1^{i}	2.864(7)
In2–O1^{iv}	2.209(5)		
In2–O1	2.209(5)		

(i) $-x+2, y, -z$; (ii) $-x+1, y, -z$; (iii) $x, y, z-1$; (iv) $x, -y+1, -z$; (v) $-x+2, -y+1, z$; (vi) $-x+\frac{3}{2}, -y+\frac{3}{2}, z$.

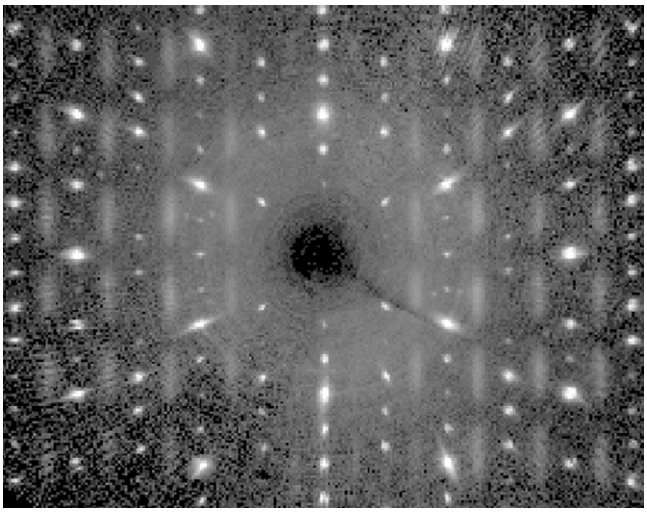

Fig. 1. *hk*0 reciprocal plane of the sublattice.

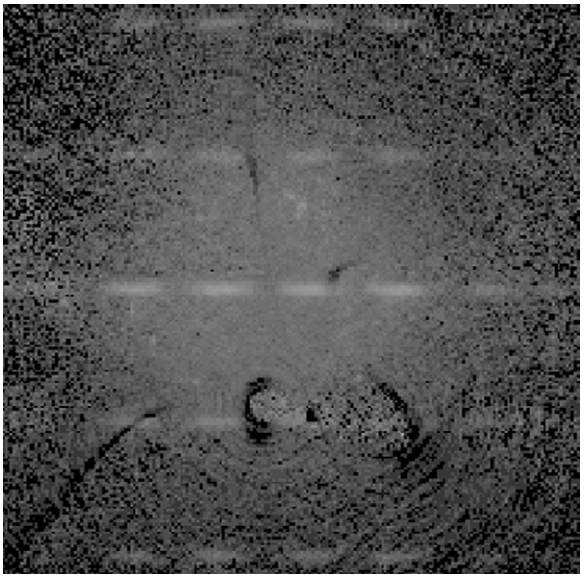

Fig. 2. 1.5*kl* reciprocal diffuse plane showing the dashed lines of diffuse spots.

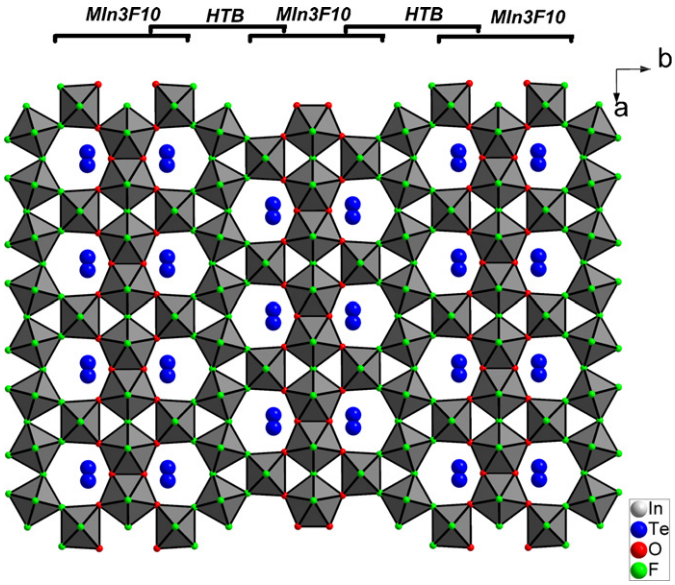

Fig. 4. Projection onto (0 0 1) plane of the two dimensional network of In polyhedra with Te cations occupying the tunnels.

substructure and trying to determine, as well as possible, a defect model able to explain the main features of the superstructure.

3. Results and discussion

3.1. Basic structure description

In the $In_3TeO_3F_7$ structure, indium cations are in six- and seven-fold coordination, in agreement with the crystal chemistry of this trivalent cation, e.g. in MIn_3F_{10} series (M = Rb, Cs, Tl, NH_4) [11] and $Ba_5In_3F_{19}$ [12].

The $In1^{3+}$cation is surrounded by four fluoride and two oxygen atoms forming an almost perfect InO_2F_4 octahedron (Fig. 3a). Each $In2^{3+}$ cation forms an InO_4F_3 pentagonal bipyramid (Fig. 3b). The $In3^{3+}$ ion occupies the centre of an almost perfect InF_6 octahedron (Fig. 3c). The main interatomic distances are given in Table 4.

Two basic units can be distinguished in this structure and refer to two different structural types. The first consists of the association of four polyhedra: two $In2O_4F_3$ pentagonal bipyramids linked by F5 vertices and sharing O1 corners with two $In1O_2F_4$ octahedra. These units share (O2–O2) edges to form strips parallel to [1 0 0] (Fig. 4). Similar strips constitute the basis of the MIn_3F_{10} and $NaM^{II}Zr_2F_{11}$ [13] structures.

The second unit consists of chains of $In3F_6$ tilted octahedra sharing F4 corners along [1 0 0]. Associated to the first basic units along [0 1 0] (Fig. 4), they constitute the 2/3 of an hexagonal tungsten bronze (*HTB*) layer. This last structure is formed by the stacking of six corner-shared WO_6 octahedra enclosing an hexagonal tunnel which can be occupied by an extra cation. In $In_3TeO_3F_7$, two of the six octahedra are replaced by two pentagonal bipyramids sharing an edge (Fig. 4). The angles In1–F6–In3 = 150.9(5)° and In3–F4–In3 = 146.6(7)° are comparable to W–O–W = 150° [14].

The strips of both substructures alternate by sharing vertices along [0 1 0] to give a host framework enclosing one-dimensional tunnels of almost hexagonal section (Fig. 4). The $In_3TeO_3F_7$ structure can then be considered as resulting from the intergrowth of MIn_3F_{10} and *HTB* structures. The indium cations form a mixed $[(3.6.3.6)^2.(3^2.6^2)]$ plane net associating two types of regular plane nets: 3.6.3.6 and $3^2.6^2$ [15].

The tellurium cations are inserted inside these tunnels and are delocalized from their centre towards the side occupied by oxygen atoms. This phenomenon can be explained by the activity of the lone pair E of tellurium IV and is also observed in the $MTeF_5$ ($M = K^+$, Na^+, Rb^+, Cs^+, Tl^+ and NH_4^+) [16] phases in which tellurium atoms are not in the centre of anionic cubes but shifted towards one of the square faces.

In $In_3TeO_3F_7$ structure, the tellurium site is very close to a mirror plane so that its symmetric site is at only 0.888 Å. The two sites have the same energy and the same anionic environment but cannot be occupied simultaneously. The Te1 cations and, by extension, the hexagonal tunnels form a semi-regular $3^3.4^2$ plane net [15], inter-

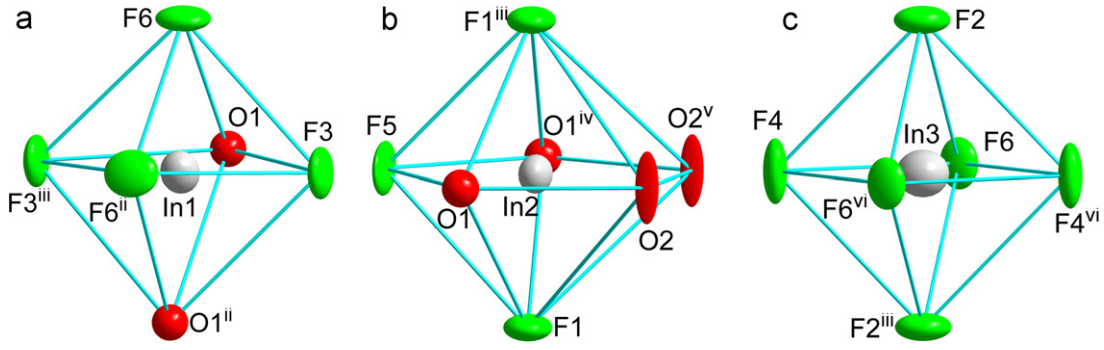

Fig. 3. Anionic polyhedra of: (a) $In1^{3+}$ [symmetry codes: (ii) $-x+1, y, -z$; (iii) $x, y, z-1$]. (b) $In2^{3+}$ [symmetry codes: (iii) $x, y, z-1$; (iv) $x, -y+1, -z$; (v) $-x+2, -y+1, z$]. (c) $In3^{3+}$ [symmetry codes: (iii) $x, y, z-1$; $-x+(3/2), (-y+(3/2)), z$].

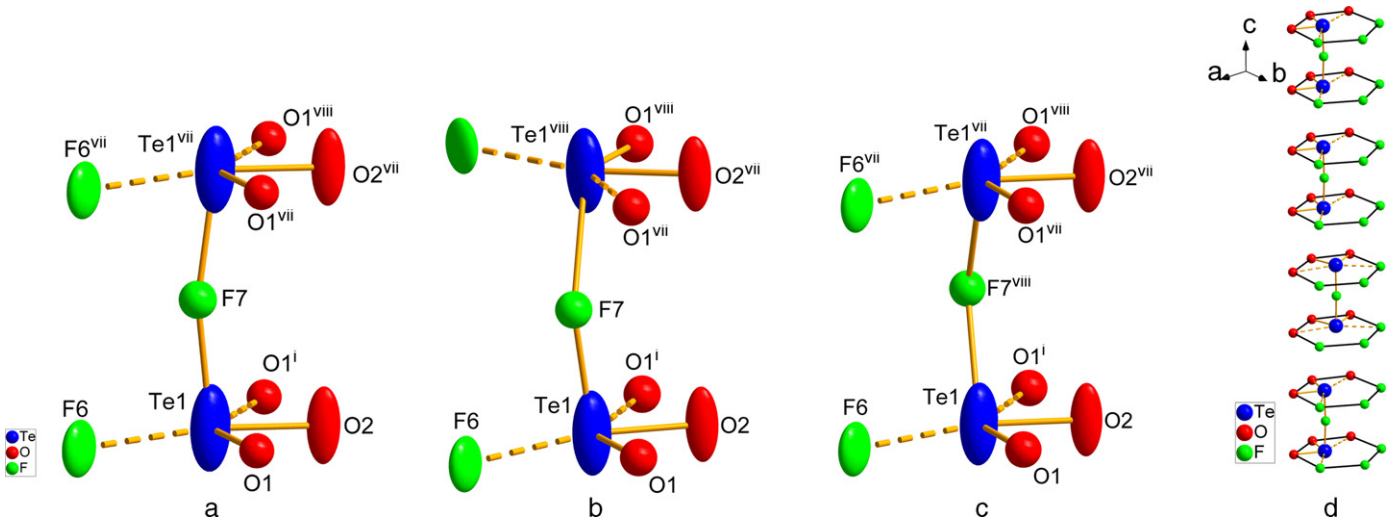

Fig. 5. Several models of short range order of the atoms Te and F inside the tunnels: (a) the tellurium cations Te1 and the fluoride anion (F7) occupy the sites of the same side of the mirror. (b) One tellurium and the fluoride atoms occupy the sites of one side of the mirror and the second tellurium occupies the site of the other side. (c) The two tellurium atoms occupy the sites of the first side of the mirror and the fluoride one occupies the site of the second side. (d) A simplified model of the tellurium atoms inside the tunnels. [Symmetry codes : (i) $-x+2, y, -z$; (vii) $x, y, z+1$; (viii) $-x+2, y, -z+1$].

mediate between 3^6 and 4^4 triangular and square regular plane nets respectively.

3.2. Short range order of Te1 and F7 in hexagonal tunnels

Each tellurium atom is strongly bonded to two oxygen atoms O1 and O2 occupying two vertices of the hexagonal section of the tunnel and to a fluoride anion F7 inserted in the tunnel. Two additional anions $O1^i$ and F6, occupying two other vertices of the hexagonal section of the tunnel can be added to the tellurium atom environment at longer distances (Table 4). The F7 anions and the Te1 cations statistically occupy two different sites, both close to the (0 1 0) mirror plane with short distances: F7–F7 = 1.11(5) Å and Te1–Te1 = 0.888(6) Å. Therefore, Te1 site is half-occupied but F7 one is only quarter-occupied. Then, there is only one F7 anion available for two Te1 cations, which is necessarily located between these two cations. Considering the splitting of the Te1 and F7 sites, several models of short range order can be imagined, from the statistical structure, to describe the local structure inside the tunnels. The $[Te_2O_4F]^-$ bipolyhedra can be linear or angulated. The linear ones are lined up parallel to [0 0 1] and occupy one or the other side of the mirror plane (Fig. 5a) and the angulated ones with Te1 and/or F7 atoms occupy both sides of the mirror plane (Fig. 5b and c). However, the most probable arrangement consists of linear bipolyhedra occupying in a disordered way one side or the other of the mirror plane (Fig. 5d). This last model leads to the better agreement in bond valence calculations (Table 5) and gives more regular Te1 polyhedra and more logical interatomic distances than the other ones. Similar bipolyhedra have already been described in a few number of bronze-related structures also containing a lone pair cation: Te^{4+} or Sb^{3+} inside hexagonal tunnels: $Sb_{0.16}WO_3$ [17], $TeMo_5O_{16}$ [18] and $Sb_2Mo_{10}O_{31}$ [19].

Table 5
Bond valence calculations for $In_3TeO_3F_7$.

Atoms	In1	In2	In3	Te1	γ_{ij}
O1	2 × 0.679	2 × 0.436		0.883/0.091	2.09
O2		2 × 0.467		1.570	2.50
F1		2 × 0.497			0.99
F2			2 × 0.499		1.00
F3	2 × 0496				0.99
F4			2 × 0.502		1.00
F5		0.456			0.91
F6	2 × 0.441		2 × 0.506	0.091	1.04
F7				0.761	1.52
γ_{ij}	3.23	3.26	3.01	3.40	

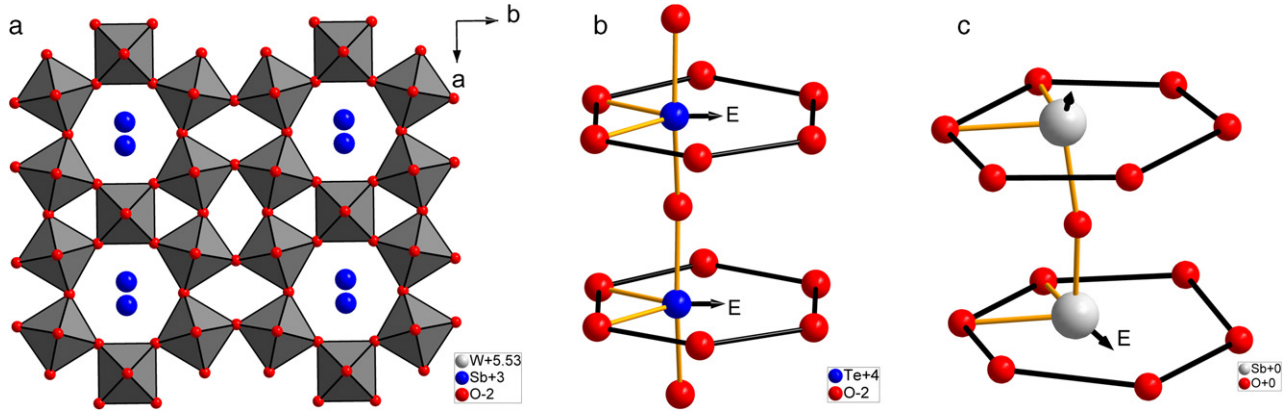

Fig. 6. Several configurations of cations with lone pairs E inside hexagonal tunnels: (a) comparison between Sb^{3+} in $Sb_{0.16}WO_3$ an Te^{4+} in $In_3TeO_3F_7$; (b and c) connectivity of Te^{4+} and Sb^{3+} inside the tunnels in $TeMo_5O_{16}$ and $Sb_2Mo_{10}O_{31}$ respectively.

The structure of $Sb_{0.16}WO_3$ is an intergrowth tungsten bronze (*ITB*) characterized by parallel slabs of *HTB* and perovskite types. Inside the hexagonal tunnel, the Sb^{3+} cation occupies the same position as Te^{4+} in $In_3TeO_3F_7$, split over two sites symmetrically shifted from the centre of the tunnel on each side of the mirror plane (Fig. 6a). A complex superstructure has also been revealed, qualitatively explained by a partially ordered distribution of the Sb^{3+} cations on these split sites.

$TeMo_5O_{16}$ (orthorhombic variety) and $Sb_2Mo_{10}O_{31}$ structures are also based on quite similar *ITB* planes but with a filling of the hexagonal tunnels by [Te–O] and [E–Sb–O–Sb–E] chains respectively (Fig. 6b and c). This last configuration corresponds to the first short range order model proposed in Fig. 5a for Te1 and F7 in a linear $[Te_2O_4F]^-$ bipolyhedron.

At this stage of the refinement, some residual electronic density ($\Delta\rho_1 = 5.62\,e\,Å^{-3}$ and $\Delta\rho_2 = 2.91\,e\,Å^{-3}$) remains near Te1 and F7 sites respectively. The first peak is at 1.98 Å from O1 and 2.02 Å from F6. The second is at 2.16 Å and 2.44 Å from Te1 and O2 respectively. These distances are in agreement with theoretical ones. In these conditions, $R_1 = 0.046$ and $wR_2 = 0.100$. The treatment of these residual electronic densities as extra Te2 and F8 sites respectively gives: $R_1 = 0.028$ and $wR_2 = 0.058$ with much lower residues of electronic density ($\Delta\rho_{max} = 2.15\,e\,Å^{-3}$ and $\Delta\rho_{min} = -1.09\,e\,Å^{-3}$).

The presence of these Te2 and F8 sites, weakly occupied, can likely be explained by more complex chain associations of Te polyhedra as proposed in Fig. 5, in which a slight shift of Te1 and F7 sites in respectively Te2 and F8 ones should occur. The final refinement has taken into account this hypothesis in correlating the occupancy rate of the mutually incompatible Te1–Te2 and F7–F8 sites in order to obtain a full occupancy for the sum of their respective amount.

3.3. O/F order

The bond valences are calculated by the Brown's method [20] and illustrated in Table 5. A perfect O/F ordering is present on the anionic sites. It is well correlated to the position of the Te1(Te2) cations. Indeed, these last atoms are systematically closer to the three O anions and conversely farer from the three F ones composing the six vertices of the hexagonal tunnel section at the same z level. As each Te1 cation is strongly bonded to two of these three O anions, two equivalent positions are possible for each Te1 cation as above discussed.

3.4. Diffuse superstructure: models of medium range order

Considering that the *a* parameter is unambiguously doubled, after the diffuse superlattice planes (see Section 2) and that the *Cmmm* space group is likely unchanged in the superlattice, half mirror planes perpendicular to [1 0 0] disappear, letting virtually unchanged the In skeleton but not the Te1(Te2) and F7(F8) framework. The main cause for the existence of a superlattice is likely the loss of the statistical character of Te1 and F7 positions which in the superlattice are likely long range ordered along [1 0 0] direction. Fig. 7 shows how, in a row of hexagonal tunnels along the [1 0 0] direction, the successive shift of $[Te_2O_4F]^-$ bipolyhedra leads to a doubling of the *a* parameter, using the *Cmmm* space group. The presence of extensive diffusion of the spots along [0 1 0] (Fig. 2) can be rationalized in the following way: if the Te1–Te1 distances are relatively long and regular along [1 0 0], extending from 6.90 to 8.91 Å, two different kinds of Te1–Te1 distances are present along [0 1 0], long ones for which two Te1 cations are separated by a $In3F_6$ octahedron (8.43–9.27 Å) and shorter ones (5.94, 6.01 Å), for which these cations are only separated by an O2–O2 edge connecting two $In2F_3O_4$ pentagonal bipyramids (Fig. 7).

The long range ordering between $[Te_2O_4F]^-$ bipolyhedra, more or less strictly established along [1 0 0], is likely rather strict between the closest Te1 bipolyhedra along [0 1 0] but much looser between the more distant ones. This hypothesis must, of course, be verified by more thorough calculations, made difficult by the residual disorder corresponding to the Te2 and F8 components of the Te1 and F7 sites in the tunnels. Similar superstructures are described in $Sb_{0.16}WO_3$ but not yet fully explained.

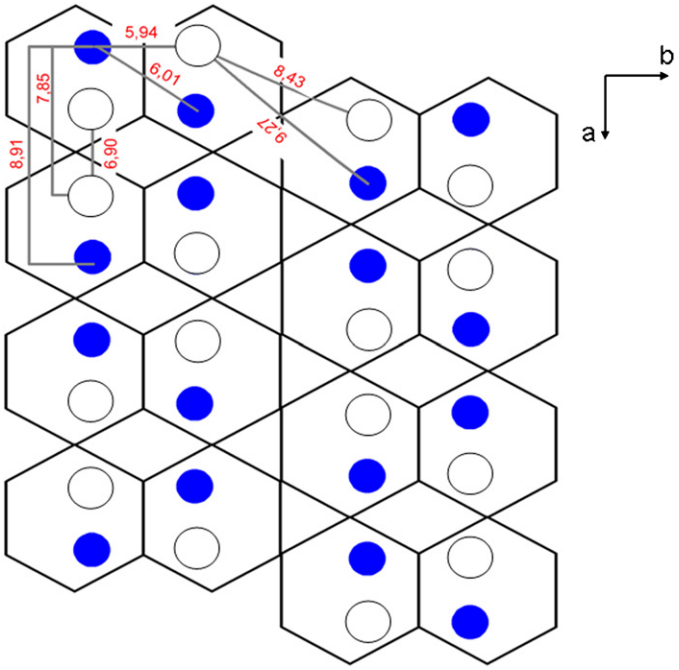

Fig. 7. Schematic representation of tellurium atoms (blue circle) ordering along [1 0 0] and [0 1 0] directions. White circles show the unoccupied tellurium sites in this model. (For interpretation of the references to colour in this figure legend, the reader is referred to the web version of the article.)

4. Conclusion

In conclusion, this new structure type is particularly interesting by the presence of Te^{4+} inside the tunnels of an hybrid structure of *HTB* and MIn_3F_{10} types. A partial ordering of the Te1 polyhedra located inside the tunnels tentatively explains the intense diffuse scattering observed. It should be interesting to approach more quantitatively the structural features of this diffuse superstructure and to try to synthesize other compounds containing lone pair cations inside cavities of such structures.

Appendix A. Supplementary data

Supplementary data associated with this article can be found, in the online version, at doi:10.1016/j.jallcom.2010.10.139.

References

[1] L. Guillet, A. Ider, J.P. Laval, B. Frit, J. Fluor. Chem. 93 (1) (1999) 33–38.
[2] A. Ider, J.P. Laval, B. Frit, J. Carré, J.P. Bastide, J. Solid State Chem. 123 (1) (1996) 68–72.
[3] J.P. Laval, N. Jennene Boukharrata, P. Thomas, Acta Crystallogr. C 64 (2008) i12–i14.
[4] J.P. Laval, N. Jennene Boukharrata, Acta Crystallogr. C 64 (2008) i57–i61.
[5] J.P. Laval, N. Jennene Boukharrata, Acta Crystallogr. C 65 (2009) i1–i6.
[6] N. Boukharrata, J.R. Duclère, J.P. Laval, P. Thomas, J. Solid State Chem., to be published.
[7] A.J.M. Duisenberg, J. Appl. Crystallogr. 25 (1992) 92–96.
[8] A.J.M. Duisenberg, L.M. Kroon-Batenburg, A.M.M. Schreurs, J. Appl. Crystallogr. 36 (2003) 220–229.
[9] Bruker, SADABS, Bruker AXS Inc., Madison, WI, USA, 2001.
[10] G.M. Sheldrick, Acta Crystallogr. A 64 (2008) 112–122.

[11] S. Aleonard, Y. Le Fur, J.C. Champarnaud-Mesjard, B. Frit, M.Th. Roux, J. Solid State Chem. 46 (1983) 87–100.
[12] A. De Kozak, N. Dupont, P. Gredin, D. Riou, Solid State Sci. 1 (1999) 409–419.
[13] M.H. Kettani, D. Avignant, J. Metin, Acta Crystallogr. C 51 (1995) 2207–2210.
[14] U. Müller, Inorganic Structural Chemistry, J. Wiley & Sons, England, 1992, p. 163.
[15] M. O'Keeffe, B.G. Hyde, Phil. Trans. R. Soc. Lond., Series A 295 (1417) (1980) 553–618.
[16] L. Guillet, PhD thesis N° 13 – 1999, University of Limoges, France, 1999.
[17] S.T. Triantafyllou, P.C. Christidis, Ch.B. Lioutas, J. Solid State Chem. 134 (1997) 344–348.
[18] P. Forestier, M. Goreaud, C. R. Acad. Sci., Paris, Serie II 312 (1991) 1141–1145.
[19] M. Parmentier, C. Gleitzer, A. Courtois, J. Protas, Acta Crystallogr. B 35 (1979) 1963–1967.
[20] I.D. Brown, in: M. O'Keeffe, A. Navrotsky (Eds.), Structure and Bonding in Crystals, vol. 2, Academic Press, New York, 1980, pp. 1–30.